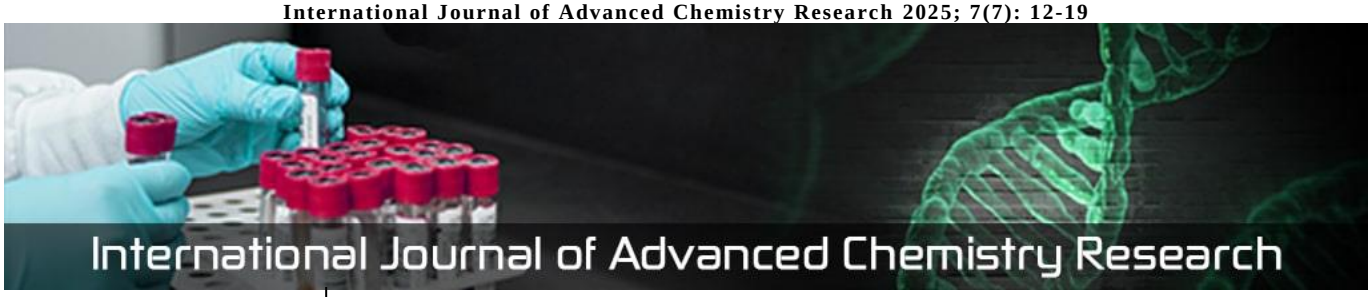

ISSN Print: 2664-6781
ISSN Online: 2664-679X
IJACR 2025; 7(7): 12-19
www.chemistryjournals.net
Received: 07-05-2025
Accepted: 09-06-2025

B Marichamy
Department of Chemistry, Mahendra Arts and Science College, Kalippatti, Namakkal, Tamil Nadu, India

S Sumitra
Department of Chemistry, Mahendra Arts and Science College, Kalippatti, Namakkal, Tamil Nadu, India

R Ajith
Department of Chemistry, Mahendra Arts and Science College, Kalippatti, Namakkal, Tamil Nadu, India

Corresponding Author:
B Marichamy
Department of Chemistry, Mahendra Arts and Science College, Kalippatti, Namakkal, Tamil Nadu, India

Synthesis, characterization and biological application of zirconiumoxide capped dihydropyrimidone derivative

B Marichamy, S Sumitra and R Ajith

DOI: https://www.doi.org/10.33545/26646781.2025.v7.i7a.295

Abstract
A new metal oxide-organic composite of Zirconiumoxide-ethyl-2-oxo-4-phenyl-1,2,34-tetrahydropyrimidine-5-carboxylate has been successfully synthesized and analyzed by elemental analysis, FT-IR, UV-Visible, GC-MS, SEM and EDAX. The biological activity of the composite has been observed by antibacterial and antifungal studies.

Keywords: Metla oxide-organic compound composite, GC-MS, EDAX, antifungal study

Introduction

Heterocyclic compounds constitute a significant portion of the biochemical materials necessary for life. Nucleic acids carry the genetic information controlling inheritance consist of long chains of heterocyclic units held together by other types of materials [1]. Spectroscopic studies of hetero cyclic compounds like those of other organic compounds, have became of great importance as means of identification of unknown materials as criteria for purity and as probes for investigating the electronic structures of molecules [2]. Biologically and pharmacologically however, the most important diazines are the pyrimidines [3]. Uracil, thymine and cytosine for example with the structures shown, are three of the five nucleotide bases that constitute the generic code in DNA and RNA [4]. Due to their biological activities heterocycles are employed in the treatment of infectious diseases [5].

The physical and chemical property of cerium oxide coated zirconium oxide (CeO_2/ZrO_2) composite was studied on cotton fabric [6]. Inorganic-organic hybrids based on zirconium peroxide (IV) and titanium isopropoxide as inorganic network precursors and N-triethylchitosan (TEC) as organic components were studied in order to control the release of NAP by encapsulation in organic-inorganic hybrids using the sol-gel technique [7]. The corrosion due to microbes was controlled by polydopamine (PDA) functionalized ceria-zirconia nanoparticles [8]. The water contamination that occurred due to methyl orange dye in the textile industry was remedied using a polyaniline-graphene oxide composite loaded with zirconium phosphate [9]. The antibacterial study was performed for ZrO_2-clay/MgO nanoparticles by using Gram-positive Bacillus subtilis and Gram-negative Pseudomonas putida [10].

In this present work, new metal oxide-organic compound composite of zirconium oxide-dihydropyrimidone derivative has been synthesized and characterized by spectral studies. Futher, biologically studied through antibacterial and antifungal activities.

2. Materials and Methods

2.1. Chemicals

Benzaldehyde, ethyl-3-oxobutanoate, urea, Zioconium oxycholoride, methanol, sulfuric acid and sodium hydroxide were purchased from Merck Chemicals.

2.2. Instrumentation

The electronic absorption was carried out by using a Shimadzu UV 1601 using ethanol as a solvent.The EQUINOX 55 Bruker spectrometer was used to obtain a spectrum of Fourier transform infra-red (FTIR). A Fourier transform infrared (FTIR) spectra was obtained on EQUINOX 55 Bruker spectrometer. The sample was prepared by grinding dried powder of ZrO2/EOPHC with KBr. The 1H spectrum was recorded on Varian Gemini Unity Spectrometer by employing TMS as internal standard. The VG AUTOSPEC mass spectrometer apparatus recorded the mass spectrum with the ESI technique. The SEM and EDX images were obtained from FEI-Quanta FEG 200F instrument. Melting point of the ZrO2/EOPHC was determined on Polmon instrument (model No.MP-96).

2.3. Biological activity

The antimicrobial tests were performed by the standard disc diffusion method. ZrO2/EOPHC has been shown to have antibacterial properties against E.coli, Pseudomonas and Klebsiella. ZrO2/EOPHC was dissolved in ethanol at concentrations of 3mg/ml was prepared. Paper discs of Whatman filter paper no. 1 were cut and sterilized in an autoclave. The paper discs were saturated with 25, 50, 75 and 100 µl of ZrO2/EOPHC composite in ethanol solution as negative control and were placed in the Petri dishes containing Nutrient agar media inoculated with the above mentioned three bacteria separately. The petridishes were incubated at 370C and the inhibition zones were recorded after 24 h of incubation. The similar procedure was followed for antifungal activity study.

2.4. Synthesis of ethyl-2-oxo-4-phenyl-1,2,3,4-tetrahydropyrimidine-5-carboxylate (EOPHC)

A solution of Urea (0.7g) and ethyl acetoacetate (1.6g) mixture was stirred for 30mins at 800C, then 1.1g of benzaldehyde was added into the round bottom flask and the reaction mixture was shaken for 1hours. After shaking the reaction mixture was kept in water bath for 1 hour at 900C, then yellow colour solid was deposited inside the conical flask. Then the reaction mixture was placed in an ice bath for an hour. The crude product was separated by filtration in vaccum pump. The crude product recrystallized by ethanol and then needle shape pure product was separated out. The synthetic path to EOPHC is depicted in Scheme 1.

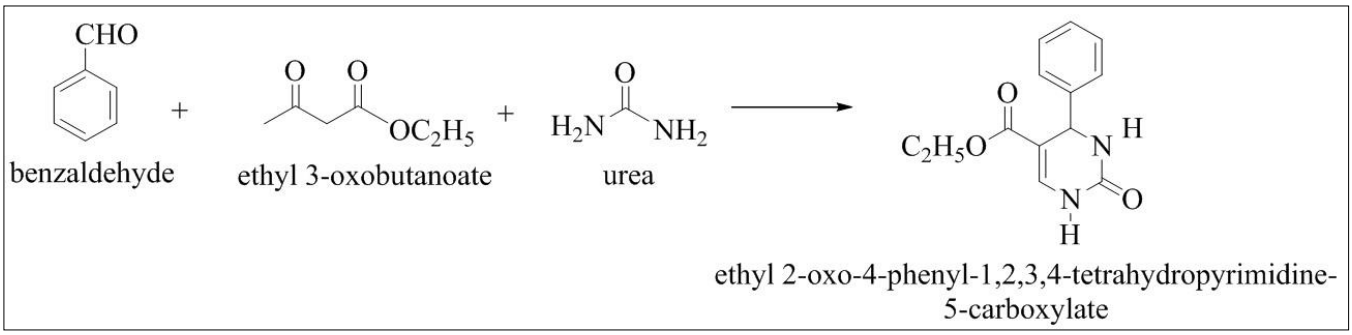

Scheme 1: Schematic diagram for synthesis of ethyl-2-oxo-4-phenyl-1,2,3,4-tetrahydropyrimidine-5-carboxylate.

2.5. Preparation of Zirconium oxide-ethyl-2-oxo-4-phenyl-1,2,3,4-tetrahydropyrimidine-5-carboxylate (ZrO2/EOPHC)

Zirconium oxide nanoparticle was synthesized from zirconyl oxychloride by addition of ammonium hydroxide [11]. Zirconium oxide nanoparticle was dissolved in 1%HCl solution, then sodium acetate (1g) and glacial acetic acid mixture (5ml) was stirred for 1hr, then the solution of EOPHC was added. Then the solution was heated at 900C for 30 min and poured into ice cold water. The pale-yellow color ZrO2/EOPHC composite was formed, then the composite has been filtered and dried. Yeild 36.2%, mp 147-1530C. IR Spectrum, cm-1: 545, 613, 767, 1091, 1222, 1300, 1595, 1712, 2882, 2939, 3240. 1H NMR spectrum (500MHz, CDCl3), δ, ppm: 3.7 s (3H), 4.92 s (1H), 6.9 d (1H, J=6.8 Hz), 7.14 d (1H, J=7.9 Hz), 7.68 s (1H). Found, %: C 44.02; N 18.76; H 5.12; Zr 2.76. C12H13N2O4Zr. Calculated: C 44.12; N 18.42; H 5.33; Zr 2.54. GC-Mass spectrum m/z: 267 (calcd for C12H13N2O4Zr: 268)

3. Results and Discussion

3.1. UV-Vis Spectroscopy: The UV-Vis absorption spectrum of the ZrO2/EOPHC composite is measured at room temperature in concentration of 5 x 10-5M acetone solution. As depicted in Fig. 1, the UV-Vis spectrum of ZrO2/EOPHC composite possesses various absorption peaks in the range of 190-1100 nm. This spectrum exhibits a strong absorption band below 250 nm, attributed to π-π* transitions. This indicates the presence of an extended conjugated π-system, commonly associated with aromatic rings or delocalized double bonds [12]. The intense absorbance in this region suggests the compound may be useful in UV-blocking or optoelectronic materials. A secondary absorption band between 300-400 nm corresponds to n-π* transitions, which typically arise from lone pair electrons on heteroatoms like nitrogen, oxygen or sulfur [13]. This suggests the presence of functional groups such as amines, carboxylic acids, or heterocyclic structures that contribute to the compound's electronic behavior. Weak absorption bands observed between 500-800 nm may indicate charge-transfer interactions, extended conjugation. These low-energy transitions broaden the compound's spectral response and point to potential applications in dye-sensitized solar cells, photodetectors or bioimaging technologies.

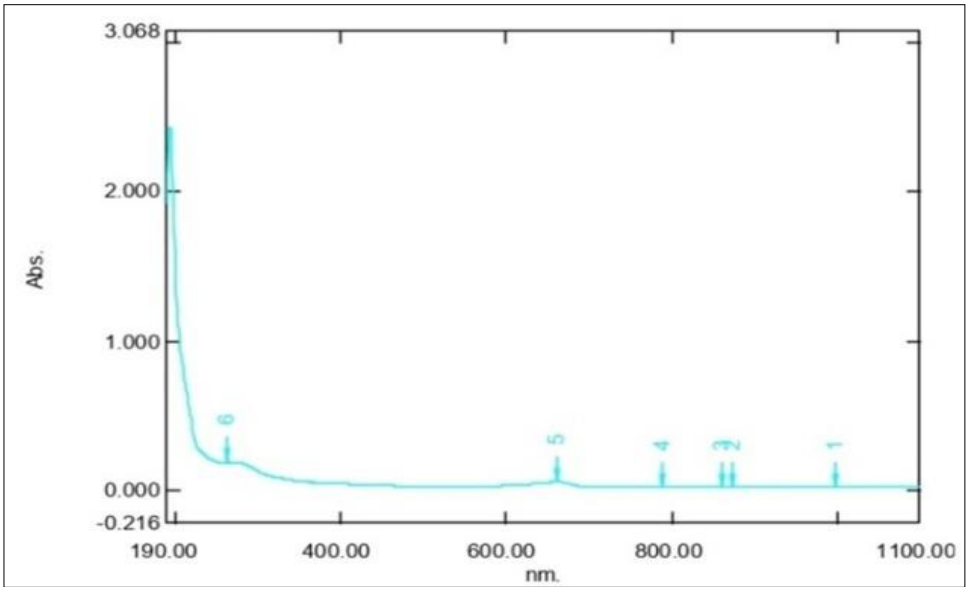

Fig 1: UV spectrum of ZrO2/EOPHC

3.2. IR Spectroscopy

The infrared spectra show that the ZrO2/EOPHC composite have different bands in the 4000-400 cm-1 (Fig. 2). A strong broad peak at 3240 cm-1 indicates -OH stretching vibrations that are indicative of alcohol [14]. C-H stretching typically observed in aliphatic hydrocarbon appears in absorption bands at 2939 cm-1 and 2882 cm-1. The presence of carbonyl group is indicated by the absorption band at 1712 cm-1 [15]. The spectrum was further analyzed with the observation of an absorption band at 1595 cm-1, attributed to C=C stretching, characteristic of the aromatic compounds. Two other peaks at 1300 cm-1 and 1222 cm-1 indicate C-N and C-O stretching, commonly found in amines, esters or ethers [16]. The absorption also at 1091 cm-1 indicate the presence of ether or alcohol functional groups. Bands at 767 cm-1 and 613 cm-1 are attributed to C-H bending vibration of aromatic rings, suggesting the presence of benzene like structures. Zr-O stretching vibration band was found at 545 cm-1 indicate that the Zr(IV) atom have bonded with oxygen atom [14].

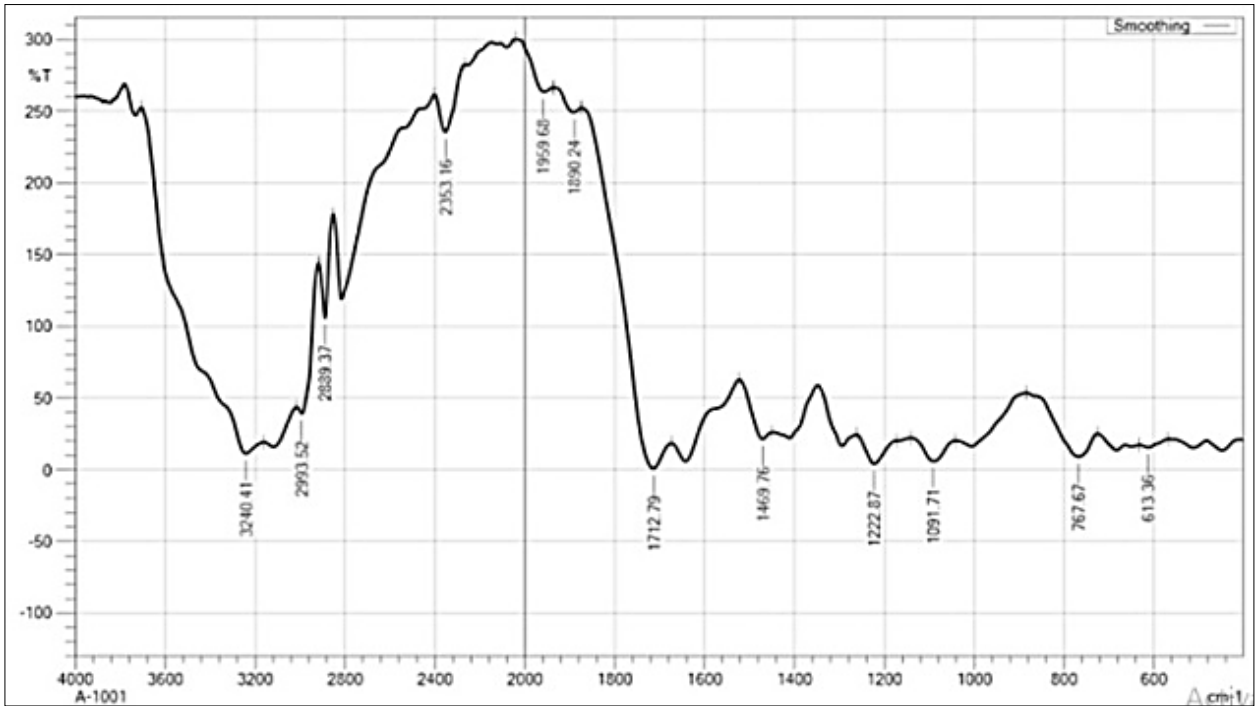

Fig 2: FTIR spectrum of ZrO2/EOPHC

3.3. NMR Spectroscopy

The 1H NMR spectra show that the ZrO2/EOPHC composite have different peaks in the 0-15 ppm (Fig.3). The peak at 6.9-7.5 ppm is suggested the presence of aromatic proton and indicates the presence of substitution occur at para position. The peak at 4.92 ppm is attributed to the presence of hydroxyl (-OH) group and peak at 3.7 ppm, which is indicated the presence of methoxy group. Peaks at 2.26 ppm and 0.82-0.85 ppm indicate the presence of methylene and methyl groups. From these values the formation of compound is confirmed [14, 15].

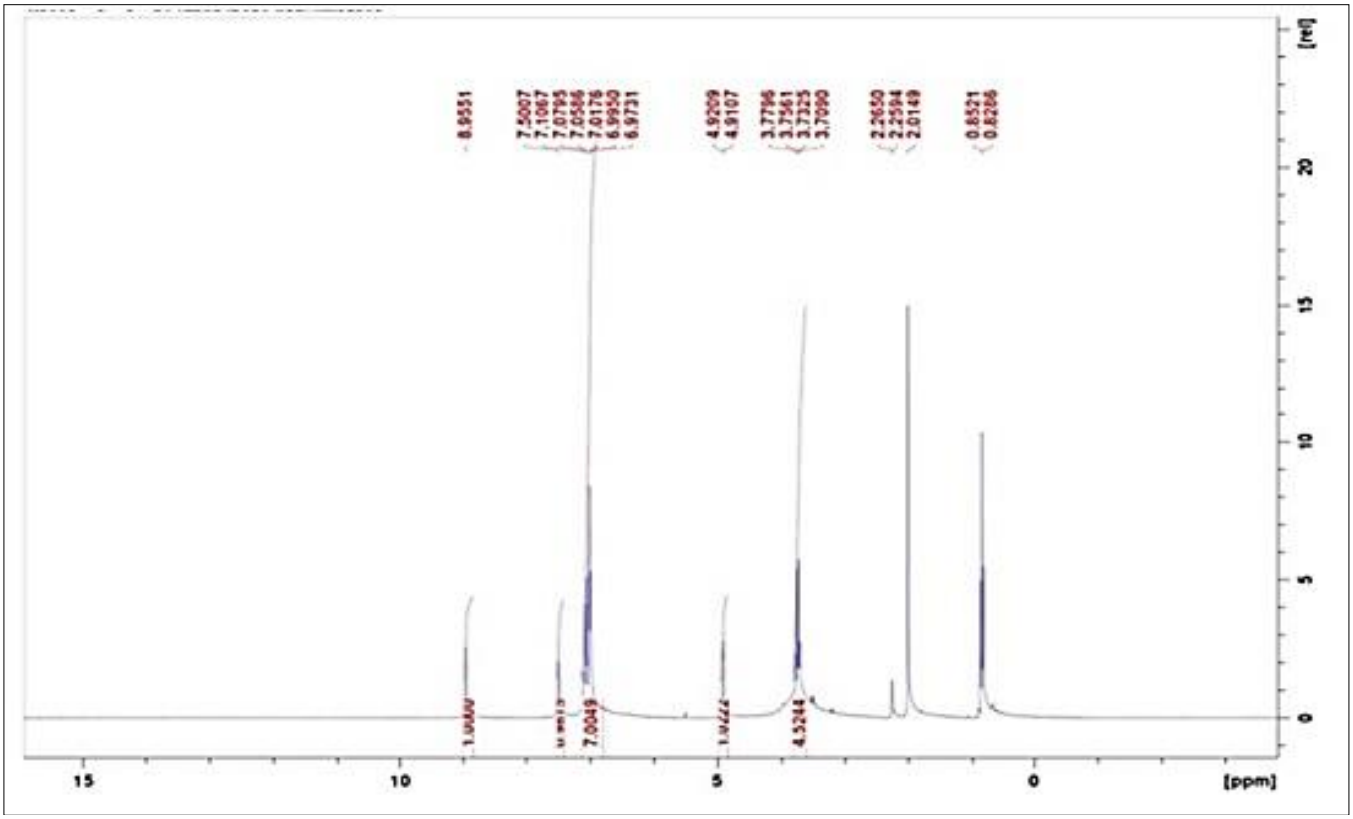

Fig 3: 1H NMR spectrum of ZrO2/EOPHC

3.4. GC-Mass Spectroscopy

The GC-MS of ZrO2/EOPHC is shown in Fig. 4.The peak at 262 (molecular ion peak) with major fragmentation peaks at m/z 247 (loss of CH3), 204, 176 consistent with the expected structure of the organic moiety, inorganic ZrO2 does not ionize but capping alters the fragmentation pattern.

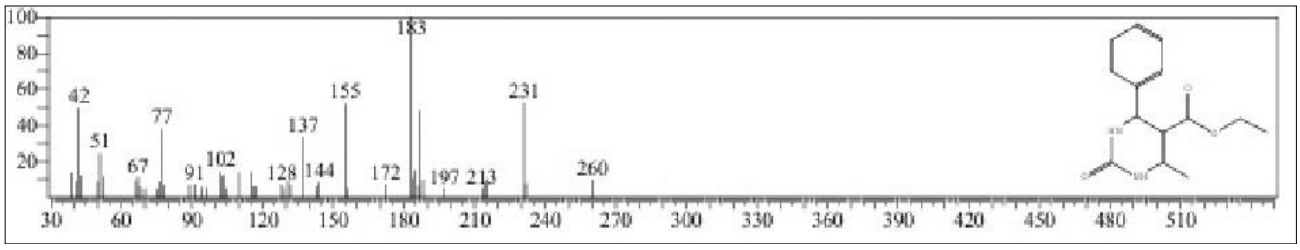

Fig 4: GC-Mass spectrum of ZrO2/EOPHC

3.5. SEM-EDX study

The SEM image of ZrO2/EOPHC is shown in Fig. 5. Aggregated particles with uneven and rough surface textures are visible in the SEM image at a 1000x magnification. A significant contact between the dihydropyrimidone moiety and the zirconium oxide nanoparticles is suggested by the nano-sized clusters, which also show a high degree of crystallinity. Partial agglomeration during synthesis or sample preparation may be the cause of the average particle size seeming to be in the micrometer to submicron range. The effective creation of a nano-hybrid material with possible functional surface properties advantageous for catalytic or medicinal applications is confirmed by this morphological investigation. Micrographs taken at 1000x and 2000x magnifications show agglomerates that are irregularly shaped and heterogeneous, with rough and flaky textures that suggest they are crystalline. Sharp-edged particles and layered structures are among the more intricate surface features seen at higher magnification (2000x), indicating a significant interaction between the organic dihydropyrimidone matrix and zirconium oxide nanoparticles [17, 18].

With some degree of particle aggregation, perhaps brought on by van der waals forces or sample drying effects, the nano zirconium oxide seems to be evenly distributed. The dihydropyrimidone derivative effective capping and stability of zirconium oxide is demonstrated by the existence of nanoscale clusters and plate-like shapes. High surface area and active site exposure are implied by these morphological traits, which are beneficial for material science, biomedical or catalysis applications. The distribution of particles indicates that the dihydropyrimidone framework effectively caps and stabilizes zirconium oxide nanoparticles adding to the surface's overall heterogeneity. The nucleation and growth dynamics during synthesis, along with the drying process, may be responsible for the rough and fragmented look.

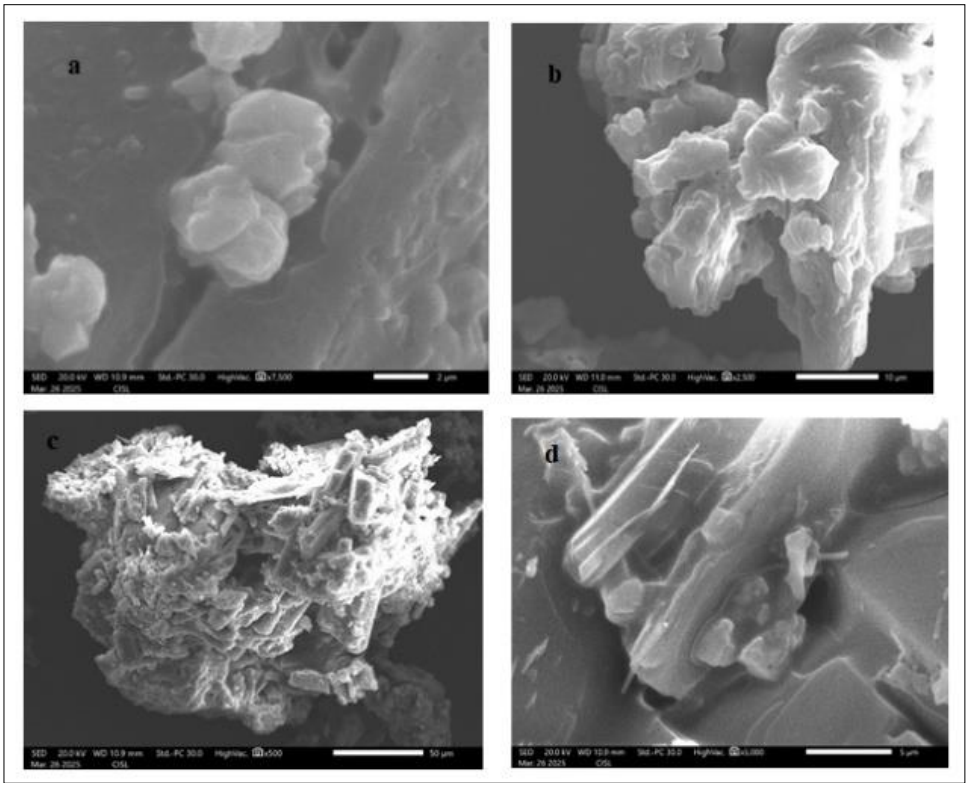

Fig 5: SEM images (a-d) of ZrO2/EOPHC

3.6. EDX Analysis: The energy-dispersive X-ray spectrum (Fig.6) identifies the presence of carbon, nitrogen, oxygen and zirconium, which are elements expected in the proposed molecular architecture. Quantitatively, carbon accounts for the highest mass percentage (44.02%), reflecting the organic backbone of the dihydropyrimidone moiety. Nitrogen (18.76%) is also prominent, consistent with the nitrogenous rings in the dihydropyrimidone core. Oxygen (34.46%) likely originates from carbonyl, hydroxyl or ether functionalities within the organic framework and potentially from coordination with zirconium atoms [17, 18].

Zirconium present at 2.76% by mass and 0.42% by atomic percentage confirms its incorporation into the compound. While the atomic percentage appears low, this is expected due to zirconium's higher atomic weight compared to the lighter organic elements. The presence of multiple zirconium peaks in the EDX spectrum, including at higher energies, further substantiates the metal's inclusion in the sample. The spatial distribution observed in the SEM image suggests that zirconium may be finely dispersed on the surface or embedded in localized regions acting as a capping or stabilizing agent for the hybrid structure. Together, the morphological and elemental data strongly support the formation of a zirconium-functionalized dihydropyrimidone derivative. The findings are consistent with a successful synthesis strategy where zirconium ions coordinate with electron-donating groups in the organic scaffold, forming a stable nano-composite material.

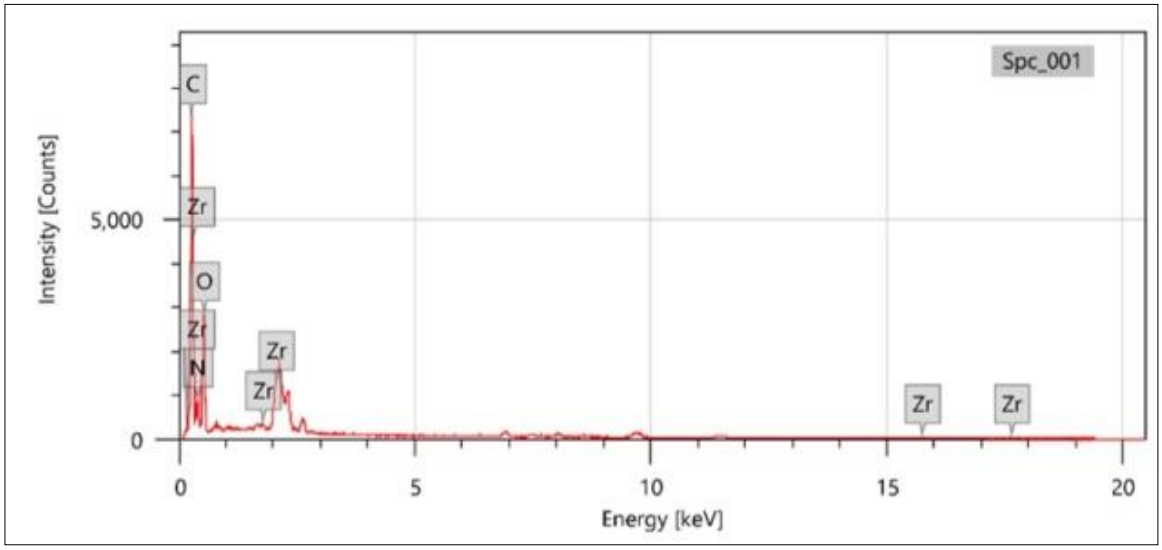

Fig 6: EDX spectrum of ZrO2/EOPHC

3.7. Anti-fungal activity

In recent investigations, zirconium oxide, a metal oxide that is both chemically stable and biocompatible, has demonstrated encouraging antibacterial properties. ZrO2 is being researched as a possible substitute for traditional antifungal drugs because of its capacity to rupture microbial cell membrane and produce reactive oxygen species. Three fungal strains Aspergillus, Mucor farreri and Candida species were used in this investigation to investigate zirconium oxide's antifungal effectiveness. The zones of inhibition at various doses (Fig. 7) were measured and tabulated (table.1) in order to evaluate the activity using the agar well diffusion technique. To assess zirconium oxide's relative potency, the outcome were contrasted with those of a common antifungal medication. ZrO2/EOPHC antifungal activity against three fungal strains Aspergillus, M far far and Candida is depicted in the bar graph (Fig. 8). Four distinct volumes of the chemical were 25 µl, 50µl, 75 µl and 100 µl. At 25 µl no inhibition was seen suggesting that the concentration was insufficient to have any antifungal effects [19, 20].

With inhibition zones of 12-14 mm, which is near the conventional drug's zone of inhibition (15mm), a modest increase in antifungal activity was observed at 50 µl. At 75 µl, the inhibitory zones grew to 19 mm for all tested fungus, indicating further improvement in activity. With inhibition zones large as 23 mm, ZrO2/EOPHC exhibited the strongest antifungal activity at the maximal volume of 100 µll. The compounds dose-dependent behavior and considered promise as an effective antifungal agent at higher concentrations were demonstrated by the fact that this exceeded the activity of the conventional antifungal medication.

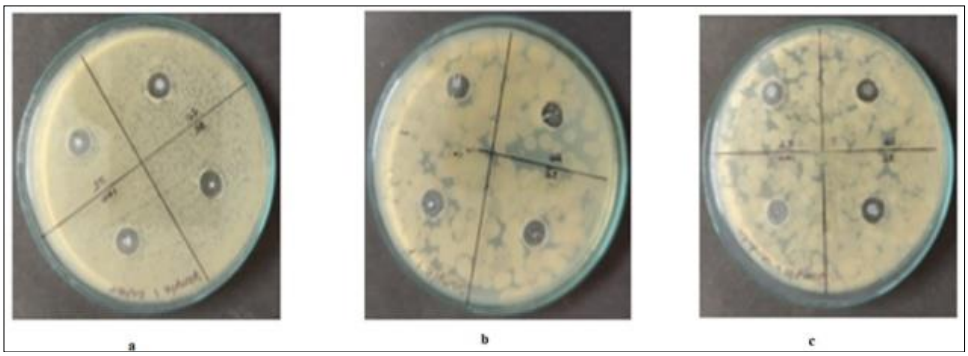

Fig 7: Anti-fungal activity images (a-c) of ZrO2/EOPHC against Aspergillus, M.far far and Candida.

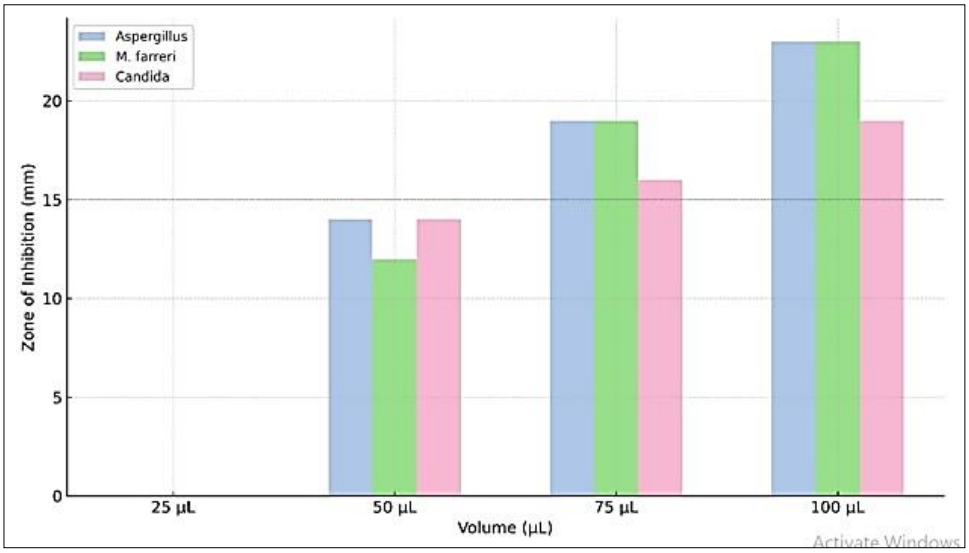

Fig 8: The bar graph for anti-fungal activity of ZrO2/EOPHC against Aspergillus, M.far far and Candida

Table 1: Anti-fungal activity of ZrO2/EOPHC against Aspergillus, M.far far and Candida

S. No	Compounds	Aspergillus (mm) M Far far(mm) Candida (mm) 25 50 75 100 25 50 75 100 25 50 75 100 µl µl µl µl µl µl µl µl µl µl µl µl
1	ZrO_2/EOPHC	Nil 14 19 23 Nil 12 19 23 Nil 14 16 19
2	Standard (25 µg/mL of methanol)	26 26 26

3.8. Anti-bacterial activity

ZrO2/EOPHC antibacterial activity (Fig. 9, 10) against three bacterial strains-Escherichia coli, Pseudomonas and Kilebsiella was evaluated and contrasted with a standard (25µl/ml in methanol). To ascertain the dose-dependent effect, varying quantities were applied during the assessment which was conducted using the agar well diffusion method [19, 20]. To assess the antibacterial efficacy, the zones of inhibition were measured in millimeters. According to the table.2, the results shows a concentration-

dependent rise in activity, especially against Pseudomonas and E.coli whereas Kilesiella shown intermediate susceptibility. A constant inhibition zone of 15 nm was shown by the standard against every strain that was tested. The potential of ZrO2/EOPHC as an antibacterial agent is highlighted by this comparative analysis particularly at higher doses.

The agar well diffusion method was employed to evaluate the antibacterial activity and dose-dependent responses were observed using varying amounts of 25, 50, 75 and 100 µl). The findings indicated that especially against E.coli and Pseudomonas exhibited increasing antibacterial activity with greater volumes, exhibiting maximum zones of inhibition at 100 µl. Kilebsiella was less sensitive yet remained responsive at greater concentrations. These results demonstrate ZrO2/EOPHC has a potential as a powerful antibacterial agent particularly at higher concentrations.

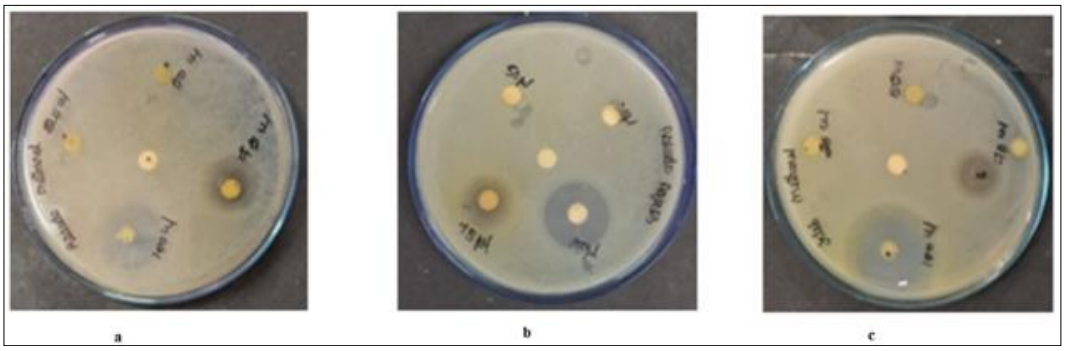

Fig 9: Anti-bacterial activity images (a-c) of ZrO2/EOPHC against Escherichia coli (E.coli), Pseudomonas species and Klebsiella species.

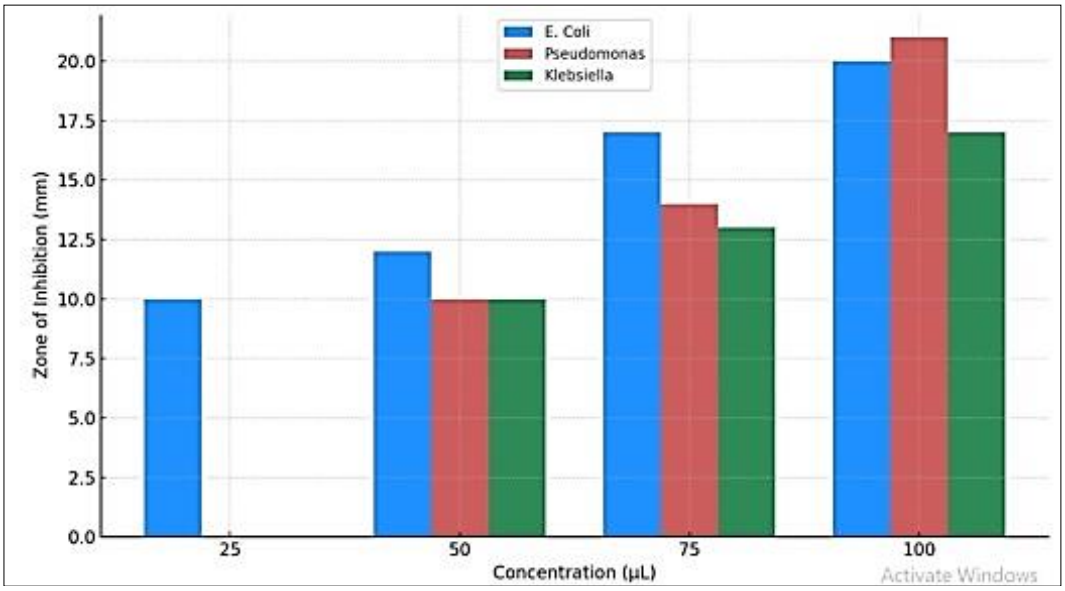

Fig 10: The bar graph for anti-bacterial activity of ZrO2/EOPHC against Escherichia coli (E.coli), Pseudomonas species and Klebsiella species.

Table 2: Anti-bacterial activity of ZrO2/EOPHC against Escherichia coli, Pseudomonas species and Klebsiella species

S.No	Compounds	E.Coli (mm) Pseudomonas (mm) Klebsiella(mm) 25 50 75 100 25 50 75 100 25 50 75 100 µl µl µl µl µl µl µl µl µl µl µl µl
1	ZrO_2/EOPHC	Nil 14 19 23 Nil 12 19 23 Nil 14 16 19
2	Standard (25 µg/mL of methanol)	26 26 26

4. Conclusion

The ZrO2/EOPHC composite was synthesized through a simple and effective method and was confirmed using various characterization techniques. UV-Vis spectroscopy showed the presence of characteristic absorption peaks, indicating the successful formation of the composite. FT-IR and NMR spectroscopy provided further structural evidence, confirming the interaction between the zirconium oxide nanoparitcle and the dihydropyrimidone moiety. SEM analysis revealed a well-defined nanoscale morphology with evenly distributed zirconium oxide particle on the organic compound, which contribute to a higher surface area and enhanced stability. The integration of nano zirconium oxide improved the thermal and chemical stability of the dihydropyrimidone structure, making it more robust under different conditions. Biological evaluation of the composite demonstrated significant antibacterial and antifungal activities, suggesting that the combination of inorganic zirconium oxide and the bioactive dihyropyrimidone enhances the overall biological effectiveness. This synergistic effect likely results from better cellular interaction and reactive oxygen species scavenging. These

findings suggest that the ZrO2/EOPHC composite has great potential for use in medical and pharmaceutical fields, such as in antimicrobial coatings, drug delivery systems or antioxidant therapies.

Acknowledgment
The authors are thankful to the TNSCST for financial support to continue this research work.

5. References

1. Maghshyam KP, Dhumal ST, Masant VH. 17-metal oxide composite in organic transformations. In: Advances in Metal Oxides and Their Composites for Emerging Applications. 2022. p. 601-632.
2. Zhang W, Abdiryin J, Jamal R. Preparation and photocatalytic activity of pendant heteroaryl groups (pyrimidine and pyridine) grafted polyterthiophene/TiO_2 composites. Mater Express. 2020;10(11):1877-1891.
3. Kumar P, Tomar V, Kumar D. Magnetically active iron oxide nanoparticles for catalysis of organic transformations: a review. Tetrahedron. 2022;106:132641.
4. Elwaky HM, Shaaban MR. Synthesis of heterocycles catalysed by iron oxide nanoparticles. Heterocycles. 2017;94(4):595-655.
5. Xia T, Shan L, Qichen. Metal composites based on pyrimidine-functionalized covalent organic frameworks and their catalytic performance. Mater Lett. 2022;327:133065.
6. Ding J, Zhang X, Chen H. Fabrication and oil-water separation properties of cerium oxide coated zirconium oxide composite membranes. Colloids Surf A Physicochem Eng Asp. 2024;683:133069.
7. Zhang Z, Zhang Y, Wang O, Ahmad I. Characterization and performance evaluation of pH-sensitive, drug delivery of nanoparticles prepared using green method with coating and capsule structure. J Mol Liq. 2024;397:124145.
8. Vijayan AS, Joseph A, Joseph A, Abhijith TS, Nair BG, Sajith V. Polydopamine functionalized ceria-zirconia nanoparticles embedded water-borne epoxy nanocomposite for anti-biofouling coatings. Prog Org Coat. 2024;187:108094.
9. Valsalakumar VC, Sreevalli Y, Archana PK, Joseph AS, Ubaid S, Vasudevan S. Removal of anionic dye from textile effluent using zirconium phosphate loaded polyaniline-graphene oxide composite: Lab to pilot scale evaluation. J Environ Manage. 2024;368:122068.
10. Bouras D, Fellah M, Barille R, Obrosov A, El Hiti GA. Production of novel Zr-Mg nanoceramics based on kaoline clay with strong antibacterial activity. Ceram Int. 2024;50:27949.
11. Wang MI, Liu BL, Shih ZW. Sol synthesis of the precursor of zirconium oxide in citric acid-ammonia solution. Chem Eng Commun. 2007;178:21.
12. Boukazoula S, Haffar D, Bourzami R, Toukal L, Dorcet V. Synthesis, characterizations, crystal structure, inhibition effects and theoretical study of novel Schiff base on the corrosion of carbon steel in 1M HCl. J Mol Struct. 2022;1261:132852.
13. Han XJ, Li RY, Yue YN, Zhang Y, Dong WK. Studying anion-dependent paradoxically fluorescent Cu(II) complexes bearing a pyridine-decorated tetradentate half-salamo-like ligand. Inorg Chim Acta. 2022;529:120634.
14. Li SZ, Tong L, Li X, Dong WK. New insight into two penta-coordinated multinuclear copper(II) single-armed salamo-based complexes. Inorg Chim Acta. 2022;540:121047.
15. Dou L, Tong L, Yan YB, Deng YH, Dong WK. Experimental and theoretical study of a sandwich-like phenoxo-bridged heterobimetallic zinc(II)-manganese(III) 3-MeOSalphen complex. J Struct Chem. 2022;63:1242.
16. Li X, Feng SS, Wei YX, Dong WK. An investigation of a relatively rigid acyclic salamo-type ligand and its square planar Cu(II) complex. J Coord Chem. 2022;75:2245.
17. Abdi J, Yahyanezhad M, Sakhaie S, Vossoughi M, Alemzadeh I. Synthesis of porous TiO_2/ZrO_2 photocatalyst derived from zirconium metal-organic framework for degradation of organic pollutants under visible light irradiation. J Environ Chem Eng. 2019;7:103096.
18. Das RS, Warkhade SK, Kumar A, Wankhade AV. Graphene oxide-based zirconium oxide nanocomposite for enhanced visible light-driven photocatalytic activity. Res Chem Intermed. 2019;45:3699.
19. Gao Q, Zhang X, Yin W, Ma D, Xie C, Zheng L, *et al.* Functionalized MoS_2 nanovehicle with near-infrared laser-mediated nitric oxide release and photochemical activities for advanced bacterial-infected wound therapy. Small. 2018;14:1802290.
20. Luo H, Huang T, Li X, Wnag J, Lv T, Tan W, *et al.* Synergistic antibacterial and wound-healing applications of an imidazole-based porous organic polymer encapsulated silver nanoparticles composite. Microporous Mesoporous Mater. 2022;337:111925.